Soft Matter

Dynamic Article Links

Cite this: *Soft Matter*, 2012, **8**, 9617

www.rsc.org/softmatter

PAPER

GAFFlipid: a General Amber Force Field for the accurate molecular dynamics simulation of phospholipid†

Callum J. Dickson,[a] Lula Rosso,[b] Robin M. Betz,[c] Ross C. Walker[cd] and Ian R. Gould*[a]

Received 30th April 2012, Accepted 20th July 2012
DOI: 10.1039/c2sm26007g

Previous attempts to simulate phospholipid bilayers using the General Amber Force Field (GAFF) yielded many bilayer characteristics in agreement with experiment, however when using a tensionless NPT ensemble the bilayer is seen to compress to an undesirable extent resulting in low areas per lipid and high order parameters in comparison to experiment. In this work, the GAFF Lennard-Jones parameters for the simulation of acyl chains are corrected to allow the accurate and stable simulation of pure lipid bilayers. Lipid bilayers comprised of six phospholipid types were simulated for timescales approaching a quarter of a microsecond under tensionless constant pressure conditions using Graphics Processing Units. Structural properties including area per lipid, volume per lipid, bilayer thickness, order parameter and headgroup hydration show favourable agreement with available experimental values. Expanding the system size from 72 to 288 lipids and a more experimentally realistic 2 × 288 lipid bilayer stack induces little change in the observed properties. This preliminary work is intended for combination with the new AMBER Lipid11 modular force field as part of on-going attempts to create a modular phospholipid AMBER force field allowing tensionless NPT simulations of complex lipid bilayers.

Introduction

Biological membranes surround cells, partitioning the interior of a cell from the outside environment. They are selectively permeable, effectively acting as a filter to maintain the unequal ion concentration on either side of the cell wall whilst allowing nutrients to enter the cell and waste products to leave.

These membranes are composed of different types of lipids, sterols, proteins and carbohydrates arranged within a lipid bilayer – a back-to-back arrangement of amphiphilic lipid molecules. As lipids are the predominant species making up cell membranes, pure lipid bilayers in the physiologically relevant liquid crystal phase are often used as model systems for biophysical and computational studies of cell membrane structure and behaviour. However, while experimental techniques including NMR spectroscopy, fluorescence spectroscopy, X-ray diffraction and neutron diffraction allow lipid bilayer structural data to be collected; the intrinsic disorder of the liquid crystalline phase means that some model dependence exists resulting in low-resolution data.[1]

Molecular dynamics (MD) simulations offer a detailed view of the structure and dynamics of bilayers, allowing the examination of experimental findings at the atomistic level and the testing of new hypotheses. Computational simulation may also provide data which is not experimentally available, such as the pressure profile of a membrane.[2] Lipid bilayers may be modelled using all-atom force fields, coarse-grained models or mesoscopic models.[3] The increasing simplicity of each of these representations allows longer timescales to be accessed using larger system sizes, at the cost of atomistic detail. Consequently, the more simplistic models are often used to study lipid phase transitions, while all-atom models are generally employed to study the behaviour of a lipid bilayer remaining in a single phase.

Computational atomistic modelling of lipid bilayer systems is currently used to investigate a range of biophysical processes, including the interaction of nanoparticles and drug molecules with lipid bilayers,[4–6] the inclusion of cholesterol,[7] and the insertion and behaviour of transmembrane proteins in lipid bilayers,[8,9] among numerous other applications. Whilst coarse-grain simulations are extremely useful for the study of the bulk system behaviour of lipid bilayers, the study of the interaction between a different species, such as a small molecule or protein, with a lipid bilayer may only be fully achieved using an atomistic model.

Force fields for the simulation of lipid bilayers have been undergoing much development.[10] Recent lipid bilayer

[a]*Department of Chemistry and Institute of Chemical Biology, Imperial College London, South Kensington, SW7 2AZ, UK. E-mail: i.gould@imperial.ac.uk*
[b]*Department of Neuroscience, Imperial College London, South Kensington, SW7 2AZ, UK*
[c]*San Diego Supercomputer Center, University of California San Diego, 9500 Gilman Drive MC0505, La Jolla, California, 92093-0505, USA*
[d]*Department of Chemistry and Biochemistry, University of California San Diego, 9500 Gilman Drive MC0505, La Jolla, California, 92093-0505, USA*

† Electronic supplementary information (ESI) available. See DOI: 10.1039/c2sm26007g

simulations have employed the GROMOS united-atom force field,[11] or the CHARMM all-atom force field[12] when examining bilayers remaining in a single phase throughout the course of a simulation. Very recently the first modular lipid force field, designed ultimately for the simulation of complex lipid mixtures, was released as part of the AMBER 12 package[13] and termed the AMBER Lipid11 force field.[14]

An additional all-atom force field available for biomolecular simulations, that has seen widespread use and formed the initial basis of the Lipid11 force field, is the General Amber Force Field (GAFF).[15] The General Amber Force Field, combined with the AMBER amino and nucleic acid force fields,[16,17] allows the accurate modelling of proteins and the easy insertion of small organic molecules into a system (by combining the RESP charge fitting methodology[18] with the General Amber Force Field[15]). Furthermore, by using the AMBER 12 MD software, previously unobtainable performance exceeding hundreds of nanoseconds per day can now be achieved using the GPU accelerated version of the code.[19,20] These points thus make it desirable to be able to simulate lipid bilayers in isolation or with transmembrane proteins embedded within them using a consistent AMBER force field. Such work was first attempted by Jójárt *et al.*, who found that POPC may be accurately simulated using the General Amber Force Field (GAFF) with the application of a surface tension to the bilayer.[21] Siu *et al.* found GAFF to allow the accurate simulation of DOPC lipid bilayers; however again the application of a surface tension was needed to achieve the best results.[22] Rosso and Gould simulated DOPC and DMPC bilayers composed of 72 lipids using GAFF for up to 25 ns, finding good agreement with experiment for a number of structural and dynamic properties in the absence of a surface tension, however the area per lipid was seen to drop slightly below experiment.[23] Indeed, it was later found that on doubling the simulation time to 50 ns both the DMPC and DOPC areas per lipid dropped significantly below experiment in the NPT ensemble, as illustrated in Fig. 1. It is important that the bilayer achieves stable structural properties in good agreement with experiment, regardless of simulation time or system size, since increasing either of these two variables moves the system closer to an experimental setup.

It is desirable to simulate lipid bilayers without an applied surface tension, as statistical mechanical studies suggest that the surface tension of a flat lipid bilayer is identically zero.[24] To remedy the underperformance of GAFF for the simulation of lipid bilayers, we show that it is necessary to adjust the Lennard-Jones parameters, which govern the van der Waals interactions. GAFF was originally developed by fitting bond, angle and torsion parameters to experimental or high level quantum chemical data for a range of simple organic compounds.[15] However the Lennard-Jones parameters have remained unchanged from the very first AMBER force field, which was developed for the simulation of proteins, nucleic acids and small organic molecules.[16] A number of recent studies have highlighted the need for a methodological parameterisation of Lennard-Jones parameters for organic liquids in order to improve the performance of GAFF[25,26] and we believe the GAFF Lennard-Jones parameters must be modified to accurately model the hydrophobic lipid tails.

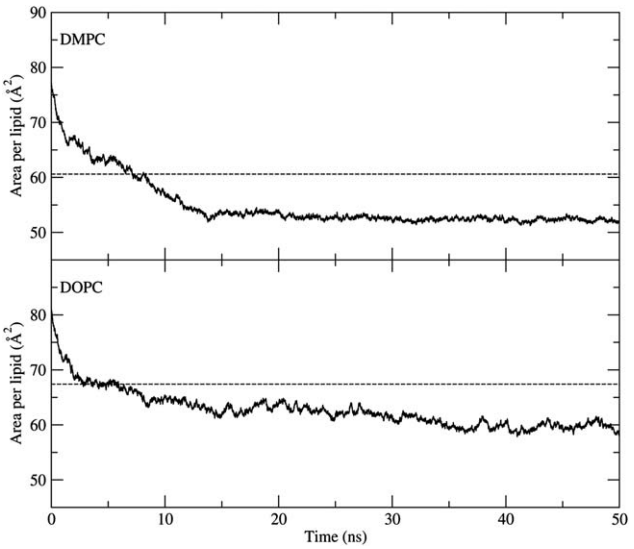

Fig. 1 Time evolution of the area per lipid for a 72DMPC and 72DOPC lipid bilayer simulated in the NPT ensemble using the standard General Amber Force Field at 303 K and hydration level of 25 waters/lipid (DMPC) and 32.8 waters/lipid (DOPC). Experimental values for DMPC[39] and DOPC[41] shown as a dashed line.

The aim of this work was to modify the General Amber Force Field to allow the accurate tensionless simulation of a number of different lipid types using AMBER; specifically lipid bilayers composed of DLPC, DMPC, DPPC, DOPC, POPC and POPE phospholipid types.

We have achieved this by refitting the Lennard-Jones parameters for acyl chain carbon and hydrogen atoms in order to replicate experimental results for simple hydrocarbon liquids. Since this impacts on the performance of torsion parameters for dihedrals involving these atom types, the torsion parameters were also re-optimised using high-level quantum chemical data in conjunction with the recently developed program Paramfit, released as part of the AmberTools12 package.[13]

The resulting parameters were then tested by simulating bilayers of each type constructed from 72 and 288 lipids and double bilayers – two 288 lipid bilayers stacked on top of one another – in the NPT ensemble and in the absence of an applied surface tension. Structural properties were then calculated for comparison with experiment. The double bilayer stack represents the lamellar stacking found in experimental studies. A similar system has previously been studied by Castro-Román *et al.* using both the CHARMM C27 and modified GROMOS lipid force field.[27]

It is hoped this work will ultimately allow the accurate simulation of lipid bilayers composed of a range of lipid types. This will mean a range of phenomena, including the properties of mixed bilayers and the behaviour of transmembrane proteins, may be investigated *via* molecular dynamics using AMBER. Although these parameters are only tested on six lipid types, it is expected that they can easily be extended to the simulation of other lipids *via* the General Amber Force Field and RESP charge fitting methodology. It is our intention to incorporate this work within the new AMBER Lipid11 modular force field,[14] to create an updated version of the Lipid11 force field allowing tensionless lipid bilayer simulations.

Methods

Modification of GAFF Lennard-Jones parameters

The General Amber Force Field is seen to underestimate the molar volume and overestimate the enthalpy of vaporisation of pentadecane, a simple fifteen carbon chain (see Table 1), suggesting the Lennard-Jones parameters for acyl chains should be corrected for such a system.

The heat of vaporisation was calculated according to:[25]

$$\Delta H_{\mathrm{vap}} = E_{\mathrm{pot}}(\mathrm{g}) - E_{\mathrm{pot}}(\mathrm{l}) + RT \quad (1)$$

This calculation involved simulating a single pentadecane molecule in the gas phase and a second simulation of a box of 144 pentadecanes in the liquid phase using AMBER 11.[28] From the second simulation the molar volume was also obtained; whilst fluctuations in the volume of the periodic box were used to calculate the isothermal compressibility value κ_{T} using:

$$\kappa_{\mathrm{T}} = \frac{{\sigma_{\mathrm{V}}}^2}{\langle V \rangle k_{\mathrm{B}} T} \quad (2)$$

where ${\sigma_{\mathrm{V}}}^2$ is the variance in the volume, $\langle V \rangle$ is the time average of the volume, k_{B} is Boltzmann's constant and T is temperature.

The gas phase simulations consisted of a single pentadecane, run for 10 ns in the microcanonical (NVE) ensemble, at a temperature of 298 K. The liquid phase simulations consisted of a box of 144 pentadecane molecules, run under the NPT ensemble with periodic boundary conditions using particle mesh Ewald to treat long range electrostatics,[29] with a real space cut-off of 10 Å. The temperature was maintained at 298 K using Langevin dynamics and a collision frequency of 5 ps^{-1}.

Pressure regulation was achieved with isotropic position scaling, a Berendsen barostat[30] and a pressure relaxation time of 1 ps. The system was heated from 0 to 298 K over 20 ps, with the chains restrained using a force constant of 20 kcal mol^{-1} $\mathrm{Å}^{-2}$. This restraint was gradually decreased to 10, 5 and finally 1 kcal mol^{-1} $\mathrm{Å}^{-2}$, with the system simulated for 20 ps for each value of the force constant. The pentadecane box was then run for 10 ns. The final 5 ns of the gas and liquid phase simulations were then used for data collection.

The CHARMM C36 lipid force field alkane carbon and hydrogen van der Waals parameters were used as a starting point for the GAFF c3 carbon and hc hydrogen atom parameters.[3] The hydrogen and carbon well-depth (ε) was then scaled (Table 2) until satisfactory agreement with experiment was achieved for molar volume, density, enthalpy of vaporisation and isothermal compressibility for pentadecane (see Table 1).

Table 2 Original and modified Lennard-Jones parameters for GAFF c3 and hc atom types

	GAFF	GAFFlipid
c3 radius R (Å)	1.9080	2.010
c3 well-depth ε (kcal mol^{-1})	0.1094	0.055
hc radius R (Å)	1.4870	1.340
hc well-depth ε (kcal mol^{-1})	0.0157	0.024

Modification of torsion parameters with Paramfit

Modification of the Lennard-Jones parameters slightly affects the performance of the torsion (or dihedral) parameters, since for atoms separated by exactly three bonds, scaled electrostatic and van der Waals interactions are calculated in addition to specific dihedral terms. This however can be easily corrected for using a new AMBER program called Paramfit.[13]

Paramfit generates or refines molecular parameters for the AMBER force field by fitting them to quantum mechanical data. It takes as input a number of conformations of the desired molecule and a topology file describing the molecular connectivity with an optional initial guess for the parameters. Paramfit will generate input files for a quantum package, which may then be used to calculate single-point energies for each of the molecular conformations using high-level quantum mechanics (QM). Given accurate parameters, the energy calculated for each structure using the AMBER equation should match the QM value for the energy of that structure within the limits of agreement possible given the restrictions imposed by the AMBER classical potential function. Paramfit optimises the parameters of the AMBER covalent terms to minimise the difference between the MD and QM energies such that:

$$\Sigma_{\mathrm{structures}}(E_{\mathrm{bonds}} + E_{\mathrm{angles}} + E_{\mathrm{dihedrals}} + E_{\mathrm{nonbond}} - E_{\mathrm{QM}} - K)^2 = 0 \quad (3)$$

for a perfect fit, where the bond, angle, dihedral and nonbonded energies are calculated as classical harmonic potentials with the AMBER equation and E_{QM} is the previously calculated quantum energy for each structure. K is a constant representing the intrinsic difference in the origin between the quantum and classical energies for the system and is used simply to rebase the calculation such that a perfect fit would give a difference of zero. The value of K has no effect on the actual fit other than to reduce round-off error when summing the small difference between a series of large numbers. It should be noted that while E_{nonbond} is included in the summation (eqn (3)), Paramfit does not attempt to adjust the parameters involved in E_{nonbond}.

Table 1 Experimental and calculated values for the enthalpy of vaporisation (ΔH_{vap}), molar volume, density and isothermal compressibility of pentadecane[a]

	ΔH_{vap} (kJ mol^{-1})	Molar volume ($\mathrm{Å}^3$)	Density (g cm^{-3})	Isothermal compressibility (10^{-10} m^2 N^{-1})
Experiment	76.77	458.99	0.769	8.82
GAFF	105.88	441.20	0.842	2.05
GAFFlipid	77.01	462.28	0.751	7.00

[a] All values at 298 K. Data taken from the CRC Handbook of Chemistry and Physics.[31]

Paramfit conducts this fitting using either a simplex or genetic algorithm. The simplex algorithm is recommended when a known parameter starting point exists; whilst the genetic algorithm is used when no good starting point exists or when coupled parameters are to be fit, such as those involving multiple dihedrals.

To correct the GAFFlipid dihedral parameters for the modified van der Waals terms a small number of torsion scans were performed on pentadecane and pentadecene molecules. The selected torsion was scanned in 15° increments at the MP4/6-311G(d,p)//MP2/6-31G* level using Gaussian 09.[32]

In this instance the simplex algorithm was used, given that only small corrections to the torsion profiles were required. Fig. 2 illustrates the ability of Paramfit to identify the torsion parameter that best replicates quantum mechanical data. The plot shows the c3–c3–c3–c3 torsion profile calculated using QM (MP4/6-311G(d,p)//MP2/6-31G* level), standard GAFF parameters, GAFF parameters in combination with modified Lennard-Jones, and finally the Paramfit corrected torsion parameters in combination with GAFF and modified Lennard-Jones. It can be seen that Paramfit brings the molecular mechanics profile into good agreement with the QM profile.

Lipid partial charges

A multi-conformer RESP fit was performed for each lipid type, using five conformations of each lipid type extracted from previous in-house bilayer simulations, affording lipid starting structures typical of the liquid crystalline phase. Each lipid molecule was optimised in the gas phase using Hartree–Fock self consistent field (HF-SCF) with the 3-21g* basis set and Gaussian 09.[32] The minimised structure then underwent further optimisation using DFT-B3LYP/3-21g* and finally HF/6-31g*. The partial charges were then extracted using the RESP protocol.

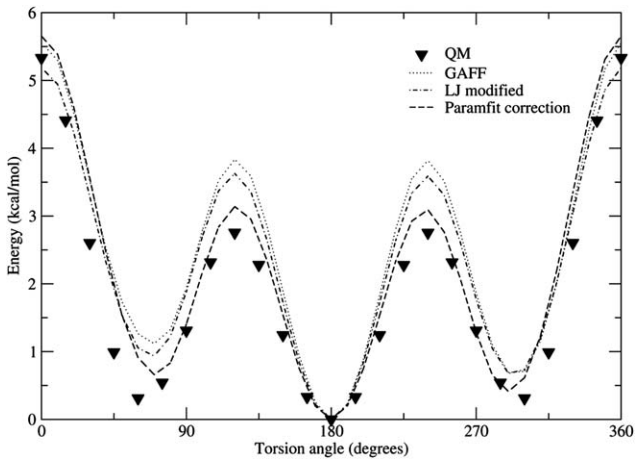

Fig. 2 Torsion profile for the CH2–CH2–CH2–CH_2 torsion (GAFF atom types c3–c3–c3–c3) calculated with a pentadecane molecule using quantum mechanics (MP4/6-311G(d,p)//MP2/6-31G* level at 15° increments), standard GAFF parameters (5° increments), GAFF parameters with modified Lennard-Jones (5° increments) and finally GAFF with modified Lennard-Jones and Paramfit corrected torsion parameter (5° increments).

The polarisable continuum model was implemented for the POPE charge calculation case to prevent proton transfer from the lipid headgroup NH_3^+ moiety to the phosphate moiety. Upon successful optimisation at this level, the partial charges were then extracted using the standard RESP protocol.

Simulation parameters are provided in full in the ESI.†

Simulation of lipid bilayers

Initial configuration. To obtain an initial configuration, a single lipid molecule was replicated along the x and y axes, and flipped along the z, until a square grid of 72 or 288 lipid molecules was obtained. A 20 Å layer of rigid TIP3P water molecules was then added above and below the bilayer using the LEAP module from the AMBER suite. Water molecules that were automatically placed below the carboxylic bonds were removed.

The 2 × 288 bilayer stacks were constructed by placing an equilibrated 288 bilayer on top of itself (with water removed) with separation so as to create a steric water thickness in line with that reported by Nagle and Tristram-Nagle,[1] then re-solvating the system with a 20 Å layer of rigid TIP3P water molecules added above and below. As with the single layer systems, water molecules that were automatically placed below the carboxylic bonds were removed.

These systems were then equilibrated using the procedure outlined in the next section, with periodic boundary conditions, a 10 Å cut-off for nonbonded (VDW and direct space electrostatics) interactions and the particle mesh Ewald summation (PME) method used to include full electrostatic interactions.[33]

Equilibration procedure. The system was first minimised with lipids constrained for 1000 steps, of which the first 250 steps used the steepest descent method and the remaining steps used the conjugate gradient method.[34] Then minimisation was performed with no restraints for 5000 steps, of which the first 2500 were steepest descent and the remaining 2500 were conjugate gradient. The system was then heated from 0 K to 303–323 K using Langevin dynamics[35] within a 20 ps constant volume run, with weak restraints on the lipid (force constant 10 kcal mol^{-1} $Å^{-2}$). Following this, the volume was allowed to change freely and the temperature kept constant with a Langevin collision frequency of $\gamma = 1.0\ ps^{-1}$, and anisotropic Berendsen control[30] of the pressure around 1 atm was applied by coupling the repeating box with a time constant of 0.5 ps for 50 ps. Finally the pressure relaxation time was reduced to 1.0 ps and the system left to equilibrate using an NPT run for 170 ps. Water was then removed from the top and bottom of the bilayers, and from below the carboxylic bonds, leaving a hydration level replicating experiment, with 31.3 waters/lipid (DLPC),[36] 25.6 waters/lipid (DMPC),[1] 30.1 waters/lipid (DPPC),[1] 32.8 waters/lipid (DOPC),[1] 31 waters/lipid (POPC)[37] or 32 waters/lipid (POPE). Each system was then equilibrated again using the same procedure.

Production runs. Constant pressure and constant temperature (NPT) runs were performed on the 72 and 288 single bilayers and the 2 × 288 bilayer stacks of DOPC, DMPC, DPPC, DLPC, POPC and POPE for simulation times of 50 ns (2 × 288 bilayers), 100 ns (288 bilayers) or 250 ns (72 bilayers) using the AMBER 11 package.[28] The CUDA implementation of the AMBER 11 code

was used to run the simulations on NVIDIA GPU cards, achieving approximately 30 ns per day for the 72 lipid bilayer systems.[19,20,28]

Three dimensional periodic boundary conditions with the usual minimum image convention were employed. Bonds involving hydrogen were constrained using the SHAKE algorithm,[38] allowing a 2 fs time-step. Structural data was recorded every 2 ps. PME was used to treat all electrostatic interactions with a real space cut-off of 10 Å. All simulations were performed at constant pressure of 1 atm and constant temperature of 303 K (DOPC, DMPC, DLPC, POPC), 310 K (POPE) or 323 K (DPPC) in order to replicate experimental conditions. Temperature was controlled by the Langevin thermostat,[35] with a collision frequency of $\gamma = 1.0\ ps^{-1}$, as this method was identified as the most suitable in previous work.[23] Pressure was controlled by the Berendsen method,[30] with a pressure relaxation time of 1.0 ps. The applied pressure was controlled anisotropically, each direction being treated independently with the trace of the pressure tensor kept constant at 1 atm. The box dimensions were thus allowed to adjust freely and independently in all three directions. The final structure of the 72DMPC, 288DMPC and 2 × 288DMPC systems are shown in Fig. 3 after completion of their respective 250 ns, 100 ns and 50 ns production runs.

Data analysis

The first 10 ns of each simulation was disregarded as equilibration time and an average value for area per lipid, volume per lipid, isothermal compressibility modulus and bilayer peak distance then computed over the entire remaining simulation. The simulation (minus equilibration period) was then divided into two equal blocks, with sub averages over each block for each property used to compute standard errors. Results in Table 3 are thus reported as average ± standard error.

Results

Structural parameters

The area per lipid is a common experimental structural parameter used in the validation of lipid bilayer simulations, however as highlighted by Poger and Mark there is often a high degree of uncertainty in experimentally derived area per lipid values.[47]

The area per lipid for each system was calculated using the dimensions of the simulation box according to:

$$A_L = \frac{2 \times L_x \times L_y}{n_{lipid}} \quad (4)$$

where L_x is the x-dimension of the simulation box, L_y is the y-dimension of the simulation box and n_{lipid} is the number of lipids in the system.

The A_L value for each system size and lipid type is reported in Table 3. It can be seen that in all cases A_L falls within 7% of experiment for all six lipid types, with little variation on increasing the system size. The time evolution of the area per lipid and comparison to experiment is also plotted in Fig. 4 for each lipid type and system size. It is seen that upon reaching equilibration the area per lipid remains stable for all systems.

The area per lipid of POPE is seen to be slightly low in comparison to experiment. The experimental value of 59–60 $Å^2$ was determined by Rappolt *et al. via* the following formula:[46]

$$A_L = \frac{2V_L}{D_{PP}} \quad (5)$$

where D_{PP} is the phosphate-to-phosphate group distance taken from the electron density profile. When this formula is applied to the modelled data, the A_L value is lower in comparison with experiment, due to a larger peak-to-peak distance in the simulated bilayers. It should also be noted that whilst there are a number of literature references for the A_L values of the other five phospholipids studied here, there remains only one literature reference point for the A_L of a pure POPE membrane.

The isothermal area compressibility modulus, K_A, was then calculated from the fluctuation in the area per lipid *via*:

$$K_A = \frac{2k_B T\langle A_L\rangle}{n_{lipid}\sigma_A{}^2} \quad (6)$$

where k_B is Boltzmann's constant, T is the temperature, $\langle A_L\rangle$ is the mean area per lipid and $\sigma_A{}^2$ is the variance in the area per lipid.

These values are also reported in Table 3 and it is observed that in general, the values for the 72 lipid bilayer systems come close

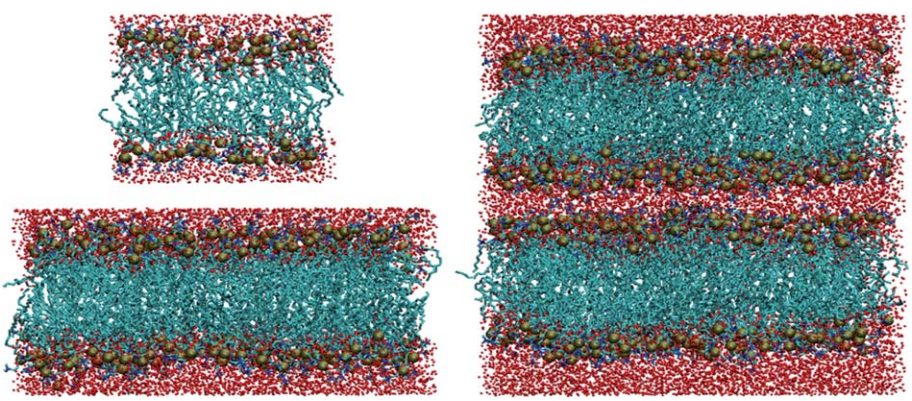

Fig. 3 Structure of the 72DMPC, 288DMPC and 2 × 288DMPC systems on completion of their respective production runs. Each system is seen to exist as a stable lipid bilayer. Choline nitrogen atoms are shown in blue; phosphate phosphorus atoms are highlighted as orange spheres; headgroup and acyl chain carbon atoms are depicted cyan; phosphate, carbonyl and water oxygen atoms are shown in red.

Table 3 Structural properties of bilayers calculated *via* molecular dynamics simulation using GAFFlipid and comparison to experiment and, where available, simulations using standard GAFF parameters, for three system sizes of six different phospholipid types

Lipid system	Area per lipid A_L (Å^2)	Volume per lipid V_L (Å^3)	Isothermal area compressibility modulus K_A (m Nm^{-1})	Peak distance D_{HH} (Å)
DLPC				
72	59.97 ± 0.0007	1008.79 ± 0.14	291 ± 64	31.6
288	60.45 ± 0.059	1009.98 ± 0.17	336 ± 7	30.6
2 × 288	62.4 ± 0.42	1007.78 ± 0.4	422 ± 297	31.5 ± 0.85
Experiment	63.2 (ref. 36)	991 (ref. 36)	—	30.8 (ref. 36)
DMPC				
72	59.95 ± 0.15	1117.83 ± 0.51	299 ± 75	33.6 ± 1
288	60.38 ± 0.0039	1115.81 ± 0.31	368 ± 74	34.6
2 × 288	61.05 ± 0.72	1105.11 ± 0.36	150 ± 150	37 ± 1
GAFF	55.8 (ref. 23)	1097.4 (ref. 23)	—	35.2 (ref. 23)
Experiment	60.6 (ref. 39)	1101 (ref. 1 and 36)	234 (ref. 40)	35.3 (ref. 39)
DPPC				
72	61.24 ± 0.4	1265.46 ± 0.8	274 ± 22	37.6 ± 0.72
288	61.77 ± 0.21	1264.51 ± 0.63	243 ± 21	37.6
2 × 288	61.75 ± 0.012	1267.24 ± 0.29	713 ± 143	39
Experiment	63 (ref. 41)	1232 (ref. 1)	231 (ref. 1)	38.3 (ref. 1)
DOPC				
72	66.79 ± 0.069	1327.41 ± 0.38	314 ± 39	37.6 ± 0.14
288	67.4 ± 0.03	1328.9 ± 0.11	392 ± 87	37.6
2 × 288	67.17 ± 0.061	1326.35 ± 0.11	1317 ± 359	38
GAFF	65, (ref. 23) 62 (ref. 22)	1333.8 (ref. 23)	—	38.4, (ref. 23) 40 (ref. 22)
Experiment	67.4, (ref. 41) 72.5 (ref. 1)	1303 (ref. 1)	254, (ref. 42) 265 (ref. 40)	35.3 (ref. 43)
POPC				
72	63.74 ± 0.22	1277.31 ± 0.16	391 ± 81	37.6
288	63.91 ± 0.059	1279.97 ± 0.15	259 ± 276	37.6 ± 0.71
2 × 288	64 ± 0.058	1276.91 ± 0.29	1147 ± 23	37.5 ± 0.5
GAFF	50.5 (ref. 21)	—	—	—
Experiment	64.3, (ref. 44) 68.3 (ref. 37)	1256 (ref. 37)	180–330 (ref. 45)	37 (ref. 37)
POPE				
72	55.64 ± 0.19	1185.21 ± 0.68	484 ± 34	43.4 ± 0.28
288	55.33 ± 0.11	1175.3 ± 0.25	282 ± 116	43.6 ± 0.41
2 × 288	56.15 ± 0.19	1185.58 ± 0.03	847 ± 244	43
Experiment	59–60 (ref. 46)	1180 (ref. 46)	—	39.5 (ref. 46)

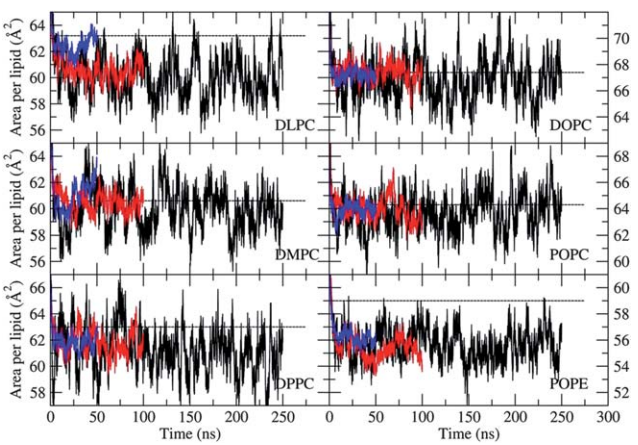

Fig. 4 Time evolution of the area per lipid for each lipid type and system size (72 bilayers black, 288 bilayers red, 2 × 288 bilayer stacks blue). Experimental values shown as a dotted line. Experimental A_L values as listed in Table 3.

to experiment, though experimental values do not always fall within the error range of the simulation values. When the system is expanded to 288 lipids and 2 × 288 bilayer stacks most calculated K_A values are seen to increase, in particular the double bilayer stacks yield very large K_A values. This is due to the low variance in A_L as can be observed in Fig. 4 (and is reflected in the low standard errors in A_L). When validating the GROMOS G53A6$_L$ lipid force field, Poger and Mark also found calculated K_A values to be sensitive both to system size and sampling time.[47]

In light of reviewers' comments, K_A was also calculated for the 2 × 288 bilayer stacks using a simplified formula which removes the dependence on n_{lipid}, the number of lipids:

$$K_A = \frac{k_B T \langle S \rangle}{\sigma_S{}^2} \quad (7)$$

where $\langle S \rangle$ is the mean surface area of the bilayer and $\sigma_S{}^2$ is the variance in the surface area. However this formula yielded the same K_A values as eqn (6), indicating that neither formula may be appropriate for stacked bilayer systems. Eqn (6) is normally applied to simulations of a single bilayer within a periodic box. It is also noted that in the current work the Berendsen barostat was implemented for pressure regulation and is in fact the only available option in AMBER, however other pressure regulation algorithms such as the Nose-Hoover[48,49] or Langevin[50] piston may yield different isothermal compressibility results.

The volume per lipid was also calculated using the dimensions of the simulation box according to:

$$V_L = \frac{V_{box} - n_W V_W}{n_{lipid}} \quad (8)$$

where V_{box} is the volume of the simulation box, n_W is the number of waters and V_W is the volume of each water molecule, which was previously determined to be 30.53 Å^3 for TIP3P water molecules.[23]

The V_L values are also reported in Table 3. Experimentally, the lipid volume shows lower fluctuation than A_L and as such is much better defined, providing a better quality experimental structural parameter with which to validate simulation results.[1,51,52] The GAFFlipid force field finds a high level of agreement with experiment for V_L values, in all instances achieving a V_L value within 2% of experiment.

Electron density profiles

The electron density profiles (EDP) were calculated by assuming an electron charge equal to the atomic number minus the partial charge of that atom, located at the centre of each atom. The total EDPs for the 72 lipid bilayers of the six lipid types are shown in Fig. 5, along with the decomposition into contributions from the following groups: water, choline (CHOL) or amine (NH_3^+), phosphate (PO_4), glycerol (GLY), carbonyl (COO), methylene (CH_2), unsaturated CH=CH and terminal methyls (CH_3). From Fig. 5 it can be seen that for each lipid type, water penetrates up to the carbonyl groups whereas the terminal methyl groups remain dehydrated, in agreement with experimental findings.[36,37,53]

From the electron density profiles, it is then possible to compute the thickness of the lipid bilayer (D_{HH}) using the peak-to-peak distance. These values are reported in Table 3. As with the A_L and V_L values, high agreement with experiment is observed for the calculated D_{HH} values for each lipid type. GAFFlipid finds D_{HH} values within 5% of experiment with the exception of the POPE model, which is within 10%. The overestimation of the POPE bilayer thickness results in the underestimated area per lipid value.

The total EDPs for each 72 lipid bilayer system were then converted into X-ray and neutron scattering form factors using the informative SIMtoEXP software developed by Kučerka *et al.*[54] The X-ray form factor, which is the Fourier transform of the total EDP, is the proper comparison for simulation since this is directly provided by experiment. The X-ray form factors are plotted in Fig. 6 while the neutron form factors are plotted in Fig. 7. Good comparison to experiment is observed for the X-ray form factors of each system; however some discrepancy is seen at low values of q for the DPPC and POPC bilayers. Each neutron form factor also displays good agreement with experiment, however again DPPC and POPC do not quite replicate the experimental profile.

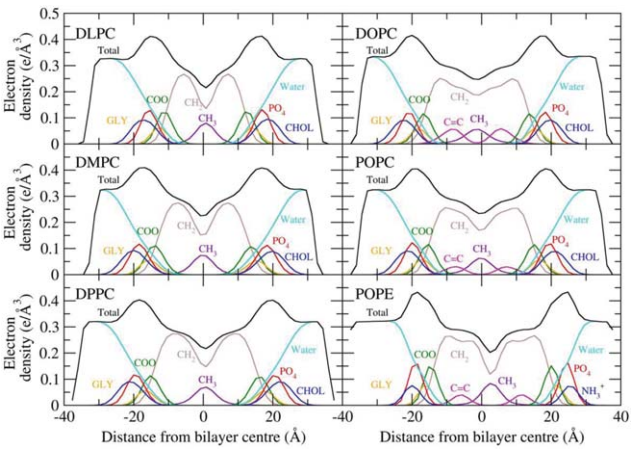

Fig. 5 The total and decomposed electron density profiles of the 72 lipid bilayer systems for each lipid type averaged over 250 ns. Contributions are shown from water, choline (CHOL) or amine (NH_3^+), phosphate (PO_4), glycerol (GLY), carbonyl (COO), methylene (CH_2), unsaturated CH=CH and terminal methyl (CH_3) groups.

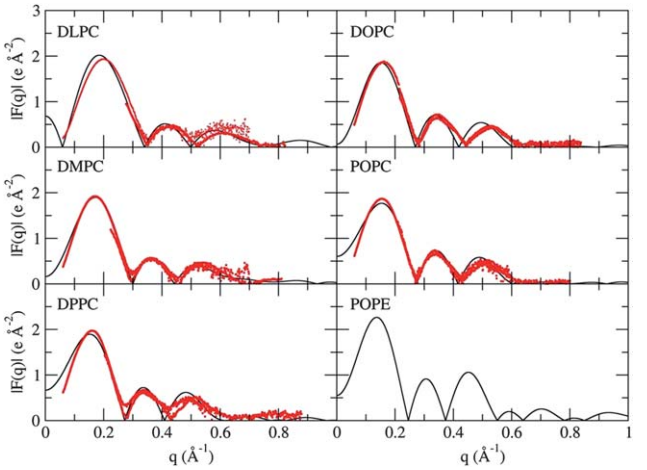

Fig. 6 X-ray form factors of the 72 lipid bilayer systems for each lipid type averaged over 250 ns (solid black line). Comparison to experiment shown (◯) for DLPC,[36,44] DMPC,[36,44] DPPC,[41,44] DOPC[42] and POPC.[37,44]

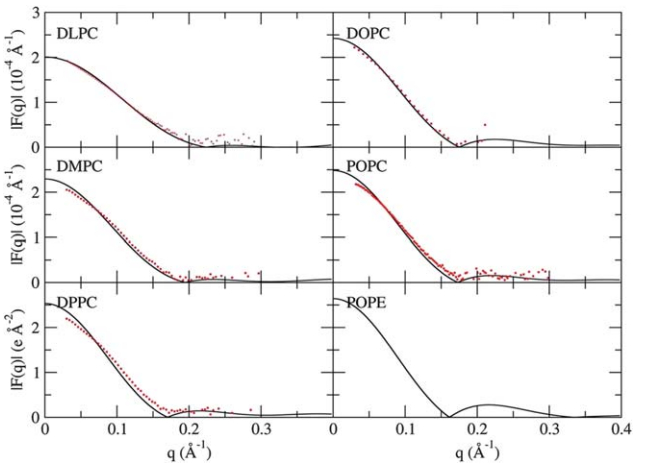

Fig. 7 Neutron form factors of the 72 lipid bilayer systems for each lipid type averaged over 250 ns (solid black line). Comparison to experiment shown (◯) for DLPC,[44] DMPC,[44] DPPC,[44] DOPC[64] and POPC.[44]

Order parameters

The order parameter S_{CD} measures the relative orientation of the C–D bonds with respect to the bilayer normal and may be calculated according to:

$$S_{CD} = \frac{1}{2}\langle 3\cos^2\theta - 1\rangle \quad (9)$$

where θ is the angle between the bilayer normal and the vector joining C_i to its deuterium atom, and $\langle\ \rangle$ represents an ensemble average.

Order parameters of the 72 and 288 lipid bilayers of the six lipid types and comparison to experiment are shown in Fig. 8. The saturated lipids DLPC, DMPC and DPPC show excellent agreement with experiment for both system sizes, exhibiting a decreasing order profile characteristic of saturated lipid chains. Carbon-2 splitting is observed in the simulation profiles, though not to the same extent observed experimentally by Douliez *et al.*[55] The unsaturated lipids DOPC and POPC also show good agreement with available experimental data. The POPE sn-1 chain order profile is higher than experiment, suggesting this chain is artificially ordered; however the sn-2 chain order profile displays a characteristic kink due to the presence of an unsaturated double bond, finding good agreement with experiment.

Given that experimental order parameter data is available for DPPC glycerol and choline carbon atoms,[56–58] the order parameter of these headgroup carbons was also calculated for the 72 DPPC bilayer system and is shown in Fig. 9 with comparison to experiment. It is seen that GAFFlipid reproduces experimental DPPC order parameter values for both the headgroup and lipid chain carbon atoms reasonably well, without adjusting headgroup torsions. Order parameter values for the first two carbon atoms in the glycerol region are slightly high; however on moving further along the headgroup better agreement with experiment is found. The largest discrepancy is the level of carbon-2 splitting, which though observed, is not to the same extent observed experimentally, as previously stated.

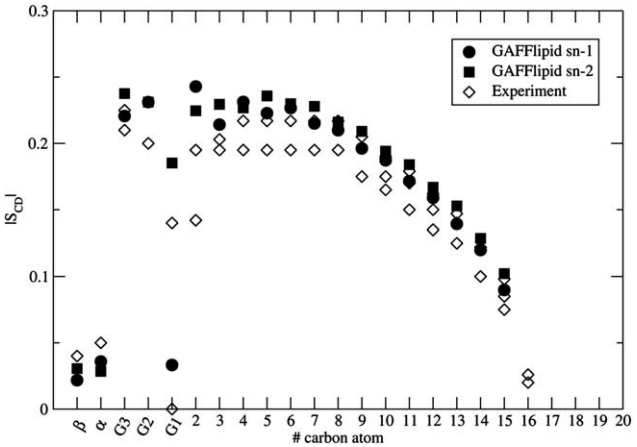

Fig. 9 Order parameter of the headgroup and lipid chain carbon atoms for the 72 DPPC system averaged over 250 ns (● sn-1, ■ sn-2) and comparison to experiment (◇).[55–58,65]

Size effects

From Table 3 it is seen that there is little change in the area per lipid, volume per lipid and bilayer thickness on quadrupling the system size from 72 to 288 lipids; or when further doubling the system size from a single 288 bilayer to a 2 × 288 bilayer stack for each lipid type. This is in agreement with Castro-Román *et al.* who observed little change in the area per lipid when expanding a DOPC bilayer in both the *xy*- and *z*-direction.[27]

Given that the experimental values were determined using lipid bilayers containing billions of lipids arranged as vertical bilayer stacks, this suggests that the GAFFlipid parameters continue to allow the stable simulation of bilayers as the system size is pushed towards that of a more realistic experimental setup, by expanding in both the *xy*- and *z*-direction.

To further investigate the effect of doubling the system size in the *z*-direction, the total electron density profiles and order parameters of the 2 × 288 bilayer stacks were also calculated for each lipid type – see Fig. 10 and 11. The order parameters are almost identical to those calculated using 72 and 288 lipid bilayers, showing similarly good agreement with experiment. A slight discrepancy is observed for the 2 × 288 DMPC bilayer stack,

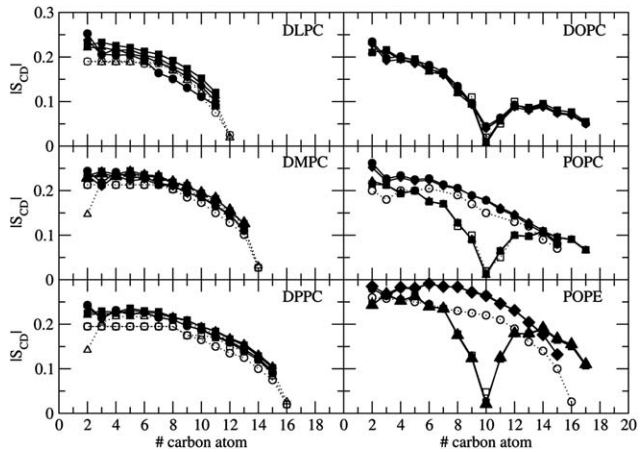

Fig. 8 Order parameters for the 72 systems averaged over 250 ns (● sn-1, ■ sn-2) and 288 systems averaged over 100 ns (◆ sn-1, ▲ sn-2) for each lipid type. Comparison to experiment shown (○ sn-1, □ and △ sn-2) for DLPC,[55,65] DMPC,[55,65] DPPC,[55,65] DOPC,[66] POPC[66,67] and POPE.[68,69]

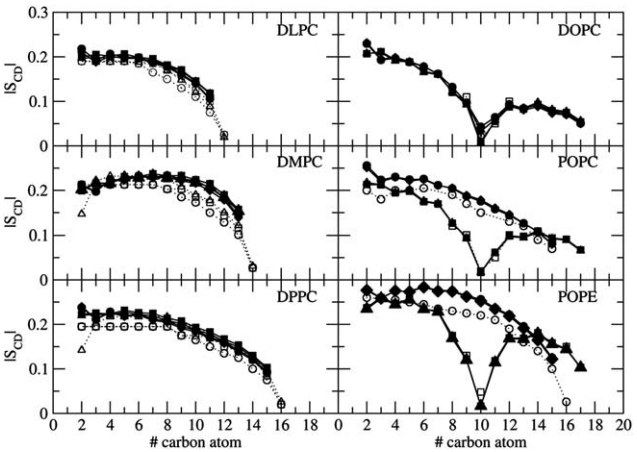

Fig. 10 Order parameters for the 2 × 288 bilayer stack systems averaged over 50 ns (lower bilayer ● sn-1, ■ sn-2; upper bilayer ◆ sn-1, ▲ sn-2) for each lipid type. Comparison to experiment shown (○ sn-1, □ and △ sn-2) for DLPC,[55,65] DMPC,[55,65] DPPC,[55,65] DOPC,[66] POPC[66,67] and POPE.[68,69]

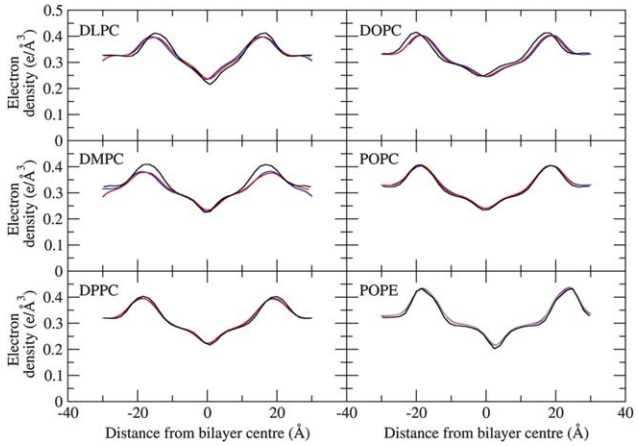

Fig. 11 Total electron density profiles for the 72 lipid bilayer systems (black) and 2 × 288 bilayer stack systems (lower bilayer blue, upper bilayer red) for each lipid type.

suggesting higher order at the tail end of the lipid chains. The total electron density profiles of the 2 × 288 systems are also seen to be very similar to those found with 72 lipid bilayers, further suggesting that finite-size effects have little influence on the lipid bilayer structural properties.

Orientation and hydration of headgroups

The probability distribution of the angle of the P–N dipole with respect to the membrane normal is plotted in Fig. 12 for each of the six lipid types. It is seen that for the five lipid types having the PC headgroup the most probable angle is approximately 60°, close to the experimental estimate of 72°,[59] and in line with the 60–90° range reported in previous lipid bilayer simulation studies.[22,47,60,61] The POPE headgroup has a tighter angle probability distribution, peaking at 68°, due to hydrogen bonding between the PE NH_3^+ moiety and the phosphate oxygen of a neighbouring lipid.[62]

The radial distribution function of the minimal distance between water oxygen atoms and the closest phospholipid

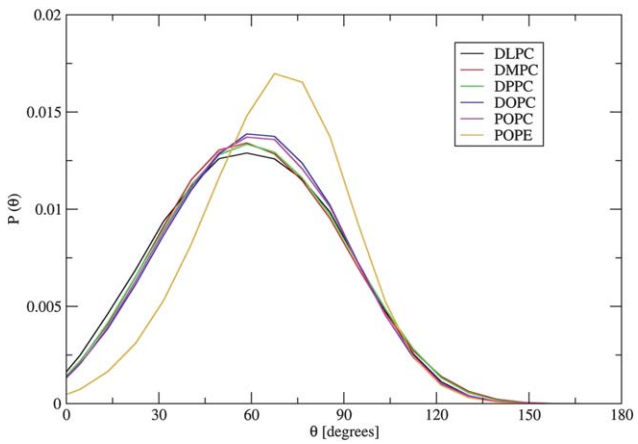

Fig. 12 Probability distribution function of the angle between the lipid headgroup P–N vector and the bilayer normal of the 72 lipid bilayer systems for each lipid type averaged over 250 ns.

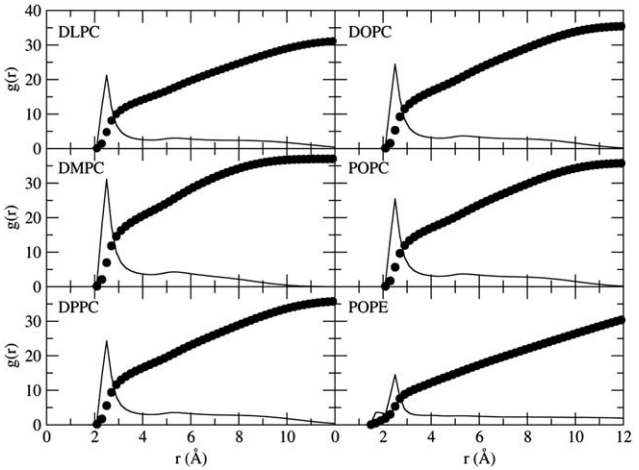

Fig. 13 Radial distribution function curves of the distance of water oxygens to the nearest lipid headgroup atom in the 72 lipid bilayer systems for each lipid type averaged over 250 ns. Integral of the distribution shown as filled black circles.

headgroup atom is shown in Fig. 13 for each lipid type. Each curve has a similar shape, with peaks at 2.52 Å and 5.31 Å, corresponding to the first and second solvation shell respectively; with the exception of the POPE plot which has an additional smaller peak at 1.73 Å corresponding to hydrogen bonding of waters to the PE NH_3^+ headgroup moiety. By integrating the water distribution it is found that in the first hydration shell there are approximately 12.04 waters (DLPC), 17.5 waters (DMPC), 14 waters (DPPC), 13.98 waters (DOPC), 14.42 waters (POPC) and 10.4 waters (POPE). These values are within the experimentally suggested range of 9–20 water molecules.[63] It is observed that the DMPC and DOPC values are higher than were previously obtained using the standard General Amber Force Field for bilayer simulation (12.5 waters for DOPC and 11 waters for DMPC),[23] however this is to be expected as the higher area per lipid values obtained in the present simulations allow greater room for hydration of the lipid headgroups.

Discussion and conclusions

Small sample size and short simulation times challenge the stability and reliability of atomistic membranes simulations. Here, the General Amber Force Field Lennard-Jones parameters, which model the van der Waals interactions within molecular dynamics simulations, have been modified for acyl chains to increase accuracy in simulation of lipid bilayers. It is shown that this modification allows a higher level of agreement between simulation and experiment for numerous structural properties, such as area per lipid, volume per lipid, bilayer thickness, order parameter and headgroup hydration to be achieved for six different lipid types. The parameters yield results that in general do not show sensitivity to increasing system size (from 72 to 288) and complexity (single bilayer to stacked configuration) and remained stable for the considerably large simulation lengths tested (50–250 ns).

Although carbon-2 splitting is observed in the order profile of the lipids studied, it is not to the same extent observed experimentally; as such this may require further investigation. The

isothermal area compressibility modulus, K_A, is reasonably well reproduced using a 72 lipid bilayer system; however, as has been previously observed, K_A is highly sensitive to increasing system size and decreasing sampling time.[47]

All systems were seen to remain stable for simulation times of up to a quarter of a microsecond. As has been found in a previous study using two different simulation packages,[27] increasing the system size in either the *xy*- or *z*-direction causes little variation in the observed structural properties. Given that there is little variation in the observed properties between a more experimentally realistic 2 × 288 bilayer system and a 72 bilayer simulated using GAFFlipid, finite-size effects do not affect the quality of the results and as such simulations using smaller bilayer patches remain valid for test purposes, provided the simulations are of an adequate duration.

These lipid simulation parameters may allow future studies such as the behaviour of membrane proteins, properties of mixed bilayers, the possible existence of lipid rafts and the interaction of small molecules, nanoparticles and antimicrobial peptides with lipid bilayers to be studied using the AMBER simulation package. Such systems are of relevance to the function and delivery of drugs; and to the workings of the cell, as cell membranes are known to exist as more than passive bystanders, rather they play an active role in the life of a cell. AMBER is particularly suited to these studies due to its atomic resolution, the easy insertion of new species into the force field, and simulation speed achievable.

Our parameters were obtained using generalised strategies – Lennard-Jones parameters were fitted to reproduce experimental data and charges and torsion parameters were derived *via ab initio* charge derivation and torsion fitting. Therefore, although this study only concerned six popular phospholipids, it is expected that they may be extended to the simulation of other lipids, such as cholesterol, sphingolipids or glycolipids; *via* GAFF and the RESP charge fitting methodology. Indeed, these parameters are intended to be incorporated with the recently released AMBER Lipid11 modular force field.[14] Lipid11 uses the standard GAFF Lennard-Jones parameters and as such requires a surface tension term for bilayer simulations; however this surface tension term may be removed once the modified Lennard-Jones parameters are adopted, providing a modularized lipid force field that can be run using a tensionless NPT ensemble.

Acknowledgements

C.J.D. thanks the Institute of Chemical Biology, UK Biotechnology and Biological Sciences Research Council (BBSRC) and GlaxoSmithKline for the award of a studentship, and the High Performance Computing centre of Imperial College London for the provision of computing time. Also thanks go to Dr Oscar Ces, Imperial College London, for useful discussions. We are extremely grateful to Professor John Nagle for helpful discussions, guidance in using the SIMtoEXP software[54] and directing us to the experimental data on the website (http://www.norbbi.com/public/public.html#Software) which we found to be an excellent resource. This work was funded in part by the National Science Foundation through the Scientific Software Innovations Institutes program – NSF SI2-SSE (NSF1047875 & NSF1148276) grants to R.C.W. and also by the University of California (UC Lab 09-LR-06-117792) grant to R.C.W. Computer time was provided by the San Diego Supercomputer Center through National Science Foundation award TGMCB090110 to R.C.W. The work was also supported by a CUDA fellowship to R.C.W. from NVIDIA. I.R.G. and R.C.W. would like to acknowledge the award of a 2010 UK-US Collaboration Development Award from the UK Foreign & Commonwealth Office, Department for Business Innovation & Skills.

References

1 J. F. Nagle and S. Tristram-Nagle, *Biochim. Biophys. Acta, Biomembr.*, 2000, **1469**, 159–195.
2 J. Gullingsrud and K. Schulten, *Biophys. J.*, 2004, **86**, 3496–3509.
3 R. W. Pastor and A. D. Mackerell Jr, *J. Phys. Chem. Lett.*, 2011, **2**, 1526–1532.
4 L. Monticelli, E. Salonen, P. C. Ke and I. Vattulainen, *Soft Matter*, 2009, **5**, 4433–4445.
5 M. Orsi and J. W. Essex, *Soft Matter*, 2010, **6**, 3797–3808.
6 A. Jusufi, R. H. DeVane, W. Shinoda and M. L. Klein, *Soft Matter*, 2011, **7**, 1139–1146.
7 M. Alwarawrah, J. Dai and J. Huang, *J. Phys. Chem. B*, 2010, **114**, 7516–7523.
8 V. Vivcharuk and Y. N. Kaznessis, *J. Phys. Chem. B*, 2011, **115**, 14704–14712.
9 A. Cordomí, G. Caltabiano and L. Pardo, *J. Chem. Theory Comput.*, 2012, **8**, 948–958.
10 A. P. Lyubartsev and A. L. Rabinovich, *Soft Matter*, 2010, **7**, 25–39.
11 D. Poger, W. F. Van Gunsteren and A. E. Mark, *J. Comput. Chem.*, 2010, **31**, 1117–1125.
12 J. B. Klauda, R. M. Venable, J. A. Freites, J. W. O'Connor, D. J. Tobias, C. Mondragon-Ramirez, I. Vorobyov, A. D. MacKerell and R. W. Pastor, *J. Phys. Chem. B*, 2010, **114**, 7830–7843.
13 D. A. Case, T. A. Darden, T. E. Cheatham III, C. L. Simmerling, J. Wang, R. E. Duke, R. Luo, R. C. Walker, W. Zhang, K. M. Merz, B. Roberts, S. Hayik, A. Roitberg, G. Seabra, J. Swails, A. W. Goetz, I. Kolossváry, K. F. Wong, F. Paesani, J. Vanicek, R. M. Wolf, J. Liu, X. Wu, S. R. Brozell, T. Steinbrecher, H. Gohlke, Q. Cai, X. Ye, J. Wang, M.-J. Hsieh, G. Cui, D. R. Roe, D. H. Mathews, M. G. Seetin, R. Salomon-Ferrer, C. Sagui, V. Babin, T. Luchko, S. Gusarov, A. Kovalenko and P. A. Kollman, *AMBER 12*, University of California, San Francisco, 2012.
14 Å. A. Skjevik, B. D. Madej, R. C. Walker and K. Teigen, *J. Phys. Chem. B*, 2012, in review.
15 J. Wang, R. M. Wolf, J. W. Caldwell, P. A. Kollman and D. A. Case, *J. Comput. Chem.*, 2004, **25**, 1157–1174.
16 W. D. Cornell, P. Cieplak, C. I. Bayly, I. R. Gould, K. M. Merz, D. M. Ferguson, D. C. Spellmeyer, T. Fox, J. W. Caldwell and P. A. Kollman, *J. Am. Chem. Soc.*, 1995, **117**, 5179–5197.
17 V. Hornak, R. Abel, A. Okur, B. Strockbine, A. Roitberg and C. Simmerling, *Proteins: Struct., Funct., Bioinf.*, 2006, **65**, 712–725.
18 C. I. Bayly, P. Cieplak, W. Cornell and P. A. Kollman, *J. Chem. Phys.*, 1993, **97**, 10269–10280.
19 A. W. Götz, M. J. Williamson, D. Xu, D. Poole, S. Le Grand and R. C. Walker, *J. Chem. Theory Comput.*, 2012, **8**, 1542–1555.
20 S. L. Grand, A. W. Götz and R. C. Walker, *Comput. Phys. Commun.*, 2012, in review.
21 B. Jójárt and T. A. Martinek, *J. Comput. Chem.*, 2007, **28**, 2051–2058.
22 S. W. Siu, R. Vacha, P. Jungwirth and R. A. Bockmann, *J. Chem. Phys.*, 2008, **128**, 125103.
23 L. Rosso and I. R. Gould, *J. Comput. Chem.*, 2008, **29**, 24–37.
24 F. Jahnig, *Biophys. J.*, 1996, **71**, 1348–1349.
25 J. Wang and T. Hou, *J. Chem. Theory Comput.*, 2011, **7**, 2151–2165.
26 C. Caleman, P. J. van Maaren, M. Hong, J. S. Hub, L. T. Costa and D. van der Spoel, *J. Chem. Theory Comput.*, 2011, **8**, 61–74.
27 F. Castro-Román, R. W. Benz, S. H. White and D. J. Tobias, *J. Phys. Chem. B*, 2006, **110**, 24157–24164.

28 D. A. Case, T. A. Darden, T. E. Cheatham III, C. L. Simmerling, J. Wang, R. E. Duke, R. Luo, R. C. Walker, W. Zhang, K. M. Merz, B. Roberts, B. Wang, S. Hayik, A. Roitberg, G. Seabra, I. Kolossváry, K. F. Wong, F. Paesani, J. Vanicek, J. Liu, X. Wu, S. R. Brozell, T. Steinbrecher, H. Gohlke, Q. Cai, X. Ye, J. Wang, M.-J. Hsieh, G. Cui, D. R. Roe, D. H. Mathews, M. G. Seetin, C. Sagui, V. Babin, T. Luchko, S. Gusarov, A. Kovalenko and P. A. Kollman, *AMBER 11*, University of California, San Francisco, 2010.
29 T. Darden, D. York and L. Pedersen, *J. Chem. Phys.*, 1993, **98**, 10089–10092.
30 H. J. C. Berendsen, J. P. M. Postma, W. F. van Gunsteren, A. DiNola and J. R. Haak, *J. Chem. Phys.*, 1984, **81**, 3684–3690.
31 W. M. Haynes, *CRC Handbook of Chemistry and Physics 92nd Edition*, CRC Press, Boca Raton, FL, 2011–2012.
32 M. J. Frisch, G. W. Trucks, H. B. Schlegel, G. E. Scuseria, M. A. Robb, J. R. Cheeseman, G. Scalmani, V. Barone, B. Mennucci, G. A. Petersson, H. Nakatsuji, M. Caricato, X. Li, H. P. Hratchian, A. F. Izmaylov, J. Bloino, G. Zheng, J. L. Sonnenberg, M. Hada, M. Ehara, K. Toyota, R. Fukuda, J. Hasegawa, M. Ishida, T. Nakajima, Y. Honda, O. Kitao, H. Nakai, T. Vreven, J. A. Montgomery, Jr, J. E. Peralta, F. Ogliaro, M. Bearpark, J. J. Heyd, E. Brothers, K. N. Kudin, V. N. Staroverov, R. Kobayashi, J. Normand, K. Raghavachari, A. Rendell, J. C. Burant, S. S. Iyengar, J. Tomasi, M. Cossi, N. Rega, N. J. Millam, M. Klene, J. E. Knox, J. B. Cross, V. Bakken, C. Adamo, J. Jaramillo, R. Gomperts, R. E. Stratmann, O. Yazyev, A. J. Austin, R. Cammi, C. Pomelli, J. W. Ochterski, R. L. Martin, K. Morokuma, V. G. Zakrzewski, G. A. Voth, P. Salvador, J. J. Dannenberg, S. Dapprich, A. D. Daniels, Ö. Farkas, J. B. Foresman, J. V. Ortiz, J. Cioslowski and D. J. Fox, *Gaussian 09*, Gaussian Inc., Wallingford CT, 2009.
33 U. Essmann, L. Perera, M. L. Berkowitz, T. Darden, H. Lee and L. G. Pedersen, *J. Chem. Phys.*, 1995, **103**, 8577–8593.
34 W. H. Press, S. A. Teukolsky, W. T. Vetterling and B. P. Flannery, *Numerical Recipes: The Art of Scientific Computing*, Cambridge University Press, New York, 2007.
35 R. Pastor, B. Brooks and A. Szabo, *Mol. Phys.*, 1988, **65**, 1409–1419.
36 N. Kučerka, Y. Liu, N. Chu, H. I. Petrache, S. Tristram-Nagle and J. F. Nagle, *Biophys. J.*, 2005, **88**, 2626–2637.
37 N. Kučerka, S. Tristram-Nagle and J. Nagle, *J. Membr. Biol.*, 2006, **208**, 193–202.
38 J.-P. Ryckaert, G. Ciccotti and H. J. C. Berendsen, *J. Comput. Phys.*, 1977, **23**, 327–341.
39 J. B. Klauda, N. Kučerka, B. R. Brooks, R. W. Pastor and J. F. Nagle, *Biophys. J.*, 2006, **90**, 2796–2807.
40 W. Rawicz, K. C. Olbrich, T. McIntosh, D. Needham and E. Evans, *Biophys. J.*, 2000, **79**, 328–339.
41 N. Kučerka, J. F. Nagle, J. N. Sachs, S. E. Feller, J. Pencer, A. Jackson and J. Katsaras, *Biophys. J.*, 2008, **95**, 2356–2367.
42 J. Pan, S. Tristram-Nagle, N. Kučerka and J. F. Nagle, *Biophys. J.*, 2008, **94**, 117–124.
43 S. Tristram-Nagle, H. I. Petrache and J. F. Nagle, *Biophys. J.*, 1998, **75**, 917–925.
44 N. Kučerka, M.-P. Nieh and J. Katsaras, *Biochim. Biophys. Acta, Biomembr.*, 2011, **1808**, 2761–2771.
45 H. Binder and K. Gawrisch, *J. Phys. Chem. B*, 2001, **105**, 12378–12390.
46 M. Rappolt, A. Hickel, F. Bringezu and K. Lohner, *Biophys. J.*, 2003, **84**, 3111–3122.
47 D. Poger and A. E. Mark, *J. Chem. Theory Comput.*, 2009, **6**, 325–336.
48 S. Nosé and M. L. Klein, *J. Chem. Phys.*, 1983, **78**, 6928–6939.
49 H. C. Andersen, *J. Chem. Phys.*, 1980, **72**, 2384–2393.
50 S. E. Feller, Y. H. Zhang, R. W. Pastor and B. R. Brooks, *J. Chem. Phys.*, 1995, **103**, 4613–4621.
51 S. C. Costigan, P. J. Booth and R. H. Templer, *Biochim. Biophys. Acta, Biomembr.*, 2000, **1468**, 41–54.
52 C. Anézo, A. H. de Vries, H.-D. Höltje, D. P. Tieleman and S.-J. Marrink, *J. Phys. Chem. B*, 2003, **107**, 9424–9433.
53 N. Kučerka, S. Tristram-Nagle and J. F. Nagle, *Biophys. J.*, 2006, **90**, L83–L85.
54 N. Kučerka, J. Katsaras and J. Nagle, *J. Membr. Biol.*, 2010, **235**, 43–50.
55 J. P. Douliez, A. Léonard and E. J. Dufourc, *Biophys. J.*, 1995, **68**, 1727–1739.
56 A. Seelig and J. Seelig, *Biochemistry*, 1974, **13**, 4839–4845.
57 A. Seelig and J. Seelig, *Biochim. Biophys. Acta, Biomembr.*, 1975, **406**, 1–5.
58 J. B. Klauda, N. V. Eldho, K. Gawrisch, B. R. Brooks and R. W. Pastor, *J. Phys. Chem. B*, 2008, **112**, 5924–5929.
59 H. Akutsu and T. Nagamori, *Biochemistry*, 1991, **30**, 4510–4516.
60 J. Taylor, N. E. Whiteford, G. Bradley and G. W. Watson, *Biochim. Biophys. Acta, Biomembr.*, 2009, **1788**, 638–649.
61 J. P. M. Jämbeck and A. P. Lyubartsev, *J. Phys. Chem. B*, 2012, **116**, 3164–3179.
62 J. M. Boggs, *Biochim. Biophys. Acta*, 1987, **906**, 353–404.
63 A. S. Ulrich and A. Watts, *Biophys. J.*, 1994, **66**, 1441–1449.
64 N. Kučerka, J. Gallová, D. Uhríková, P. Balgavý, M. Bulacu, S.-J. Marrink and J. Katsaras, *Biophys. J.*, 2009, **97**, 1926–1932.
65 H. I. Petrache, S. W. Dodd and M. F. Brown, *Biophys. J.*, 2000, **79**, 3172–3192.
66 J. Seelig and N. Waespe-Sarcevic, *Biochemistry*, 1978, **17**, 3310–3315.
67 A. Seelig and J. Seelig, *Biochemistry*, 1977, **16**, 45–50.
68 B. Perly, I. C. P. Smith and H. C. Jarrell, *Biochemistry*, 1985, **24**, 4659–4665.
69 S. R. Shaikh, M. R. Brzustowicz, N. Gustafson, W. Stillwell and S. R. Wassall, *Biochemistry*, 2002, **41**, 10593–10602.